

Automatic profile reconstruction for millimeter-wave frequency-modulated continuous-wave reflectometry on NSTX

S. Kubota,^{a)} W. A. Peebles, and X. V. Nguyen

Institute of Plasma and Fusion Research, University of California, Los Angeles, California 90095

A. L. Roquemore

Princeton Plasma Physics Laboratory, Princeton, New Jersey 08543

(Presented on 8 July 2002)

UCLA operates a set of millimeter-wave/microwave reflectometers on the National Spherical Torus Experiment (NSTX) for routine measurements of electron density profiles and fluctuations. The system has a combined frequency coverage of 12 to 50 GHz (in the bands 12–18, 20–32, and 33–50 GHz) or a corresponding ordinary-mode cutoff range of 1.8×10^{12} to 3.1×10^{13} cm⁻³ to cover both the plasma core and edge. Profile measurements via frequency-modulated continuous-wave operation are typically made in O-mode reflectometry, with sweep times down to 50 μ s over the full band. Automated profile analysis of the reflectometry data is available with limited between-shot analysis and full batch analysis capabilities. The reconstruction algorithm uses complex demodulation with the short-time Fourier transform for signal processing. The unknown portion of the edge profile below the lowest cutoff density is modeled by fitting a family of polynomial density profiles to the experimental data. Uncertainties due to edge profile modeling and comparisons to Thomson scattering measurements are discussed. The reconstructed profiles have documented fast events such as L–H transitions and edge-localized modes in NSTX. © 2003 American Institute of Physics. [DOI: 10.1063/1.1530391]

I. INTRODUCTION

Between-shot analysis with good spatial and temporal resolutions is increasingly becoming a requirement for modern fusion plasma diagnostics. In addition, simultaneous profile and fluctuation measurements are being viewed as ultimately necessary for a comprehensive understanding of turbulence and related transport. The millimeter-wave reflectometry system¹ installed at the National Spherical Torus Experiment (NSTX)² can provide either electron density profile or fluctuation measurements over a wide density range (1.8×10^{12} to 3.1×10^{13} cm⁻³) covering portions of both the plasma core ($\rho = r/a < 0.8$) and edge ($\rho > 0.8$) regions. Density profile measurements are made via frequency-modulated, continuous-wave (FM-CW) operation, while fluctuation measurements are made via fixed-, stepped-, or narrow-band swept-frequency operation of the sources.

The goal of our current work is to implement millimeter-wave FM-CW reflectometry as a standard diagnostic on NSTX in order to provide between-shot density profiles. FM-CW reflectometry is a radar technique in which the phase accumulation or time delay is measured for frequency-swept electromagnetic radiation reflected from a plasma cut-off layer.³ Although the hardware implementation can be relatively straightforward, the process of reconstructing profiles from the acquired data may be computationally challenging. Extensive digital signal processing is required to analyze the large amount of data that is acquired (48 MB per shot on NSTX). Analysis may be complicated by the effects

of signal degradation due to plasma fluctuations.⁴ In addition, further profile information in the form of the magnetic field profile for X-mode reflectometry, or the edge profile for O-mode reflectometry, is necessary. EFIT is available on NSTX,⁵ however, with the present system and magnetic field configuration, the portion of the profile below 12 GHz must still be modeled, regardless of the mode polarization.

The control and data acquisition portions of the diagnostic have performed reliably and routinely (shot-to-shot) over the past year. The article describes the software development work that has been done to provide between-shot analysis. In addition to tackling the computational difficulties mentioned earlier, the code should run autonomously with little intervention from the user. The routines that have been developed are therefore computationally intensive. Currently, data is analyzed as batch jobs during off-hours. For between-shot capability, multiple dedicated CPUs will be required. The necessary computer hardware and optimum network topology are issues that are still being studied.

The remainder of this article is structured as follows. Section II provides a brief introduction to NSTX and the diagnostic hardware. This is followed by a description of the profile reconstruction algorithm in Sec. III. Here, the details of the signal processing, edge modeling, and final inversion methods are discussed. Some experimental results are presented in Sec. IV. Comparisons are made with density profiles from Thomson scattering; examples of the profile evolution during edge-localized mode (ELM)-free and ELMy H-mode discharges are also shown. Section V concludes with a summary of the present work and our outlook for future work concerning the diagnostic.

^{a)}Electronic mail: skubota@ucla.edu

II. PLASMA DEVICE AND DIAGNOSTIC DESCRIPTIONS

NSTX is a low aspect ratio ($R/a \sim 1.3$) device with auxiliary heating due to neutral beam injection up to 7 MW and high-harmonic fast-wave injection up to 6 MW. Typical device parameters are $R_0 = 85$ cm, $a = 68$ cm, $I_p = \leq 1.5$ MA, $B_T = 0.3\text{--}0.6$ T, with $\kappa \leq 2.5$ and $\delta \leq 0.8$. Further descriptions of the device are given in Refs. 2 and 6–8.

The millimeter-wave FM-CW reflectometer on NSTX is similar in design to an existing system used for electron density profile analysis on DIII-D.^{9–11} Frequency-tunable solid-state sources in conjunction with active frequency multipliers provide a frequency range of 12 to 50 GHz, which corresponds to an O-mode cutoff range of 1.8×10^{12} to 3.1×10^{13} cm⁻³. The reflectometer is actually three similar systems in the frequency bands 12–18, 20–32, and 33–50 GHz, utilizing bistatic horns mounted internal to the vacuum vessel on midplane ports. All aspects of the data acquisition, hardware control, and system triggering can be controlled interactively by LabVIEW from anywhere on the Internet. A further description of the diagnostic can be found elsewhere.¹

In a typical operating scenario, the frequency sweep consists of multiple pairs of 50 μ s up/down sweeps. Both a monitor of the sweep pattern as well as the mixer intermediate frequency (IF) are recorded for each system at 50 MSamples/s. The mixer IF can range from 2 to 10 MHz, depending on the target (centerstack or plasma) or the density profile shape. The usual operational mode is to use the digitizers in burst mode (818 records per shot), with each record sampling a single up/down sweep pair. The interval between burst records can be varied on a shot-by-shot basis to look at the entire discharge, or the evolution of fast changes in the profile up to a maximum repetition rate of 8 kHz.

III. PROFILE RECONSTRUCTION ALGORITHM

A. Basic concepts

The phase shift ϕ_p of the reflected electromagnetic wave or probe wave due to propagation through the plasma can be written within the geometric optics approximation as¹²

$$\phi_p(f) = \frac{4\pi f}{c} \int_{r_c(f)}^{r_0} \mu(r, f) dr - \frac{\pi}{2}, \quad (1)$$

where $\mu(r, f)$ is the refractive index of the plasma, r_0 is the outer radius of the plasma, and $r_c(f)$ is the radius of the cutoff layer for a probe frequency f . Swept-frequency operation allows a series of cutoff layers (or a portion of the density profile) to be probed.

Since the probe frequency is swept in time, the mixer output has a frequency $d\phi/df$, where ϕ is the total phase difference between reference and probe paths. ϕ includes ϕ_p as well as contributions from path differences due to waveguide or cable runs, vacuum distance outside the plasma, etc. A phase calibration using the reflection from a target at a known distance in the vacuum vessel (in the case of NSTX, the centerstack) is sufficient to isolate ϕ_p .

For O-mode reflectometry, the quantity μ is a function only of density and f , hence either Eq. (1) or its Abel inversion,¹³

$$r(f_p) = r_0 - \frac{c}{\pi} \int_0^{f_p} \frac{\tau(f) df}{(f_p^2 - f^2)^{1/2}}, \quad (2)$$

can be used to determine the profile. Here $\tau(f) \equiv d\phi_p/df$ is the group delay and f_p is a chosen plasma cutoff frequency. For X-mode reflectometry, μ is also a function of the magnetic field. Reconstruction in this case requires using Eq. (1). The actual steps of the profile reconstruction algorithm follow.

B. Signal processing for complex demodulation

The accumulated phase of the mixer IF is extracted numerically using the complex demodulation (CDM) method (phase accuracy of $\leq \pi/10$).⁹ The workhorse of our implementation is the short-time Fourier transform (STFT), which is defined as¹⁴

$$X[n, \omega] = \sum_{m=-\infty}^{\infty} x[n-m] w[m] e^{-j\omega m}. \quad (3)$$

Here $X[n, \omega]$ denotes the STFT of the time series $x[n]$ multiplied by the windows sequence $w[m]$, which is a two-dimensional function of the time and frequency variables n and ω . Using a series of overlapping sum-to-one windows (such as the Hamming window), a spectrogram of the IF signal is created without loss of signal content. Frequency shifting and filtering for CDM are performed in the frequency domain for each spectrum. Key parameters are the length and number of overlaps of the window sequence, which can be adjusted for tradeoffs in computation time, frequency resolution or time resolution.

C. Smoothing over turbulence effects

The CDM analysis yields phase and amplitude traces versus time (or frequency) for each sweep. It is known from both one-dimensional and two-dimensional full-wave calculations^{4,15} that spatial and temporal plasma perturbations or turbulence can cause localized decreases and deformations (or in our case, glitches) in the reflected signal amplitude and phase or phase-derivative curve (see Fig. 1). The amplitude information is crucial, since it allows amplitude-weighted smoothing of the phase or phase-derivative signals to eliminate local deformations. Typically, the location of these deformations varies randomly from sweep to sweep, and amplitude-weighted averaging across multiple sweeps also tends to eliminate deformations.

D. Edge profile modeling

Edge modeling errors have been studied in detail,^{16,17} with the main result that errors increase for shallower gradients, however, the position error introduced by this uncertainty decreases as the density increases.

The model profiles we use is a family of polynomials of the form

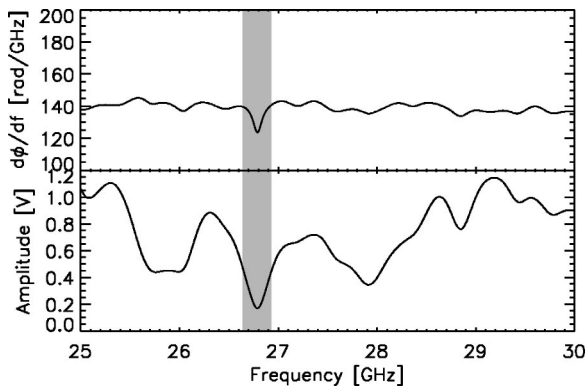


FIG. 1. Degradation of the mixer output signal due to turbulence effects. Shown are the amplitude and $d\phi/df$ curves as a function of probe frequency. Turbulence effects are manifest as sudden drops in the amplitude, which correspond to glitches in $d\phi/df$.

$$n_e(r) = n_{e1} \left[1 - \left(\frac{r-r_1}{r_0-r_1} \right)^\alpha \right]^\beta, \quad (4)$$

where r is the major radius, r_0 is the plasma edge, r_1 is the radius with density n_{e1} , and α and β are shaping parameters. The advantage of using Eq. (4) is that a solution to the integral in Eq. (1) exists in analytic form. The phase derivative can then be written¹⁸

$$\frac{d\phi_p(f)}{df} = \frac{4\pi}{c} (r_0 - r_1) \sum_{j=0}^{\infty} \frac{(j - \alpha^{-1}) \cdots (1 - \alpha^{-1}) \alpha^{-1}}{j!} \times \frac{\sqrt{\pi}}{\beta} \frac{\Gamma[(j+1)/\beta]}{\Gamma[(j+1)/\beta + 1/2]} \left(\frac{f}{f_0} \right)^{2(j+1)/\beta}. \quad (5)$$

For $\alpha=1$ and $\beta \geq 1$ Eq. (4) produces monotonically increasing profiles with a finite gradient at r_1 and zero gradient at r_0 (see Fig. 2). Usually n_1 is chosen at some value above the lowest cutoff density. The portion of the overlap for experimental and modeled $d\phi_p/df$ is evaluated for goodness of fit. Having analytic formulas for both the trial edge profiles and corresponding $d\phi_p/df$ greatly accelerates the fitting process.

E. Inversion method

The inversion method follows the procedure outlined in Refs. 19 and 20. Suppose the measurements of $\phi_{pi} = \phi_p(f_i)$ exist on a regular frequency grid $f=f_i$, i

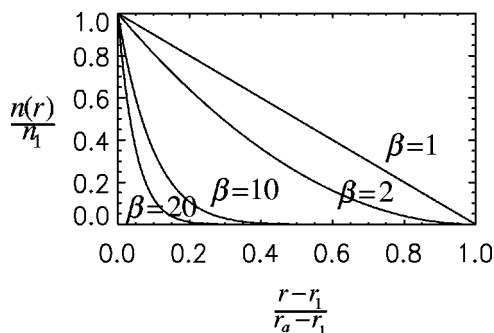


FIG. 2. Examples of the family of polynomials used to model the edge profile below the lowest cutoff density ($1.8 \times 10^{12} \text{ cm}^{-3}$).

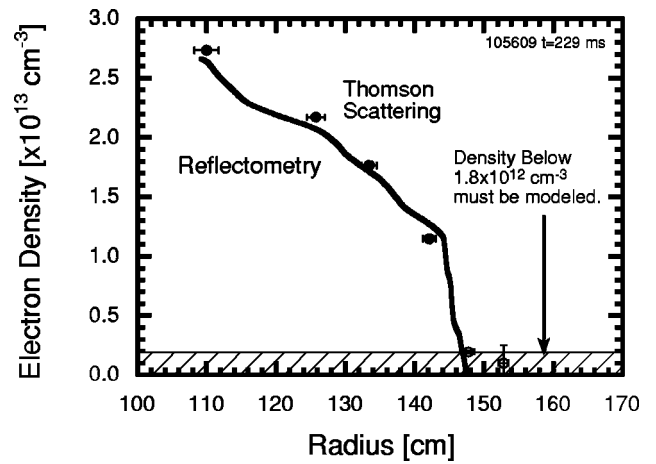


FIG. 3. Comparison of reconstructed profile with Thomson scattering profile. Typically both profiles track each other very well. Radial differences between the two profiles are usually less than $\pm 1-2$ cm.

$= 0, 1, 2, \dots, n$. If we assume linear density profiles between all successive f_i , then by defining the following quantity:

$$A_{ij} \equiv \frac{8\pi}{3c} \left[\frac{(f_i^2 - f_{j-1}^2)^{3/2} - (f_i^2 - f_j^2)^{3/2}}{(f_j^2 - f_{j-1}^2)} \right], \quad (6)$$

$$i, j = 1, 2, \dots, \text{ and } i \geq j,$$

and by ignoring the constant term, we can rewrite Eq. (1) as

$$\phi_{pi} = - \sum_{j=1}^i A_{ij} (r_j - r_{j-1}), \quad (7)$$

which can be simplified in matrix notation as

$$\begin{bmatrix} \phi_1 \\ \phi_2 \\ \phi_3 \\ \vdots \\ \phi_n \end{bmatrix} - r_0 \begin{bmatrix} A_{11} \\ A_{21} \\ A_{31} \\ \vdots \\ A_{n1} \end{bmatrix} = \begin{bmatrix} -A_{11} & 0 & 0 & \cdots \\ A_{22} - A_{21} & -A_{22} & 0 & \cdots \\ A_{32} - A_{31} & A_{33} - A_{32} & -A_{33} & \cdots \\ \vdots & \vdots & \vdots & \vdots \\ A_{n2} - A_{n1} & A_{n3} - A_{n2} & A_{n4} - A_{n3} & \cdots \end{bmatrix} \begin{bmatrix} r_1 \\ r_2 \\ r_3 \\ \vdots \\ r_n \end{bmatrix}. \quad (8)$$

Since A_{ij} and therefore the matrix on the right-hand side of Eq. (8) is not an explicit function of r , we can obtain r , by multiplying both sides by the inverse of this matrix. The advantages here are that the inversion process for each profile is reduced to a simple matrix multiplication, and for a standard grid of frequencies the inversion matrix need only be calculated once.

IV. EXPERIMENTAL RESULTS

Figure 3 shows a comparison of the reconstructed reflectometer profile with measurements from the multi-point Thomson scattering system.²¹ Typically, the two profiles track each other very well to within a radial separation of $\pm 1-2$ cm. The fact that the profiles are also near the edge

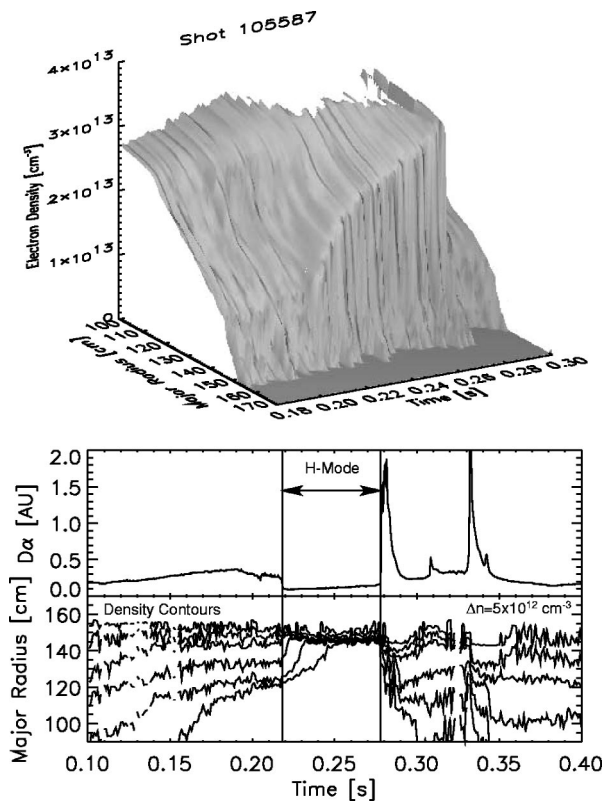


FIG. 4. Time evolution of reconstructed reflectometer profiles for an ELM-free H-mode shot. Typical of such discharges are the sudden steepening of the edge gradient at the L-H transition and the growth of the edge pedestal with time.

may indicate that the error in the reflectometer profiles due to uncertainty in the edge profile may indeed be very small.

The time evolution of the reconstructed reflectometer profile is shown in Fig. 4 for an ELM-free H-mode discharge. Characteristics of such H-mode discharges in the spherical torus are clearly evident; the sudden increase in the edge density gradient at the L- to H-mode transition, as well

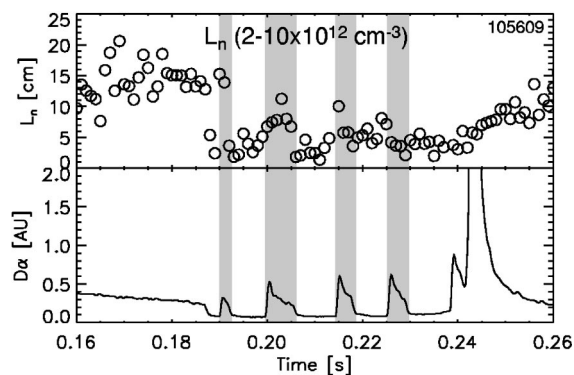


FIG. 5. Time evolution of the gradient scale length calculated from reflectometry profile data for an ELM-free H-mode discharge. Here $L_n = n/(dn/dr)$ is averaged over the section of the profile between 2×10^{12} to $1 \times 10^{13} \text{ cm}^{-3}$. For this shot the time interval between profiles is 1 ms.

as the gradual rise of the edge pedestal height, can be distinguished. Figure 5 shows the time evolution of the edge gradient scale length during an ELM-free H-mode discharge. The quantity $L_n = n/(dn/dr)$ was calculated from the reflectometer profile by averaging over the portion of the discharge between 2×10^{12} and $1 \times 10^{13} \text{ cm}^{-3}$. For this shot, the time interval between successive profiles was 1 ms. At this repetition rate one can see that the profiles do not quite catch all of the changes in the ELM profile structure.

V. SUMMARY AND FUTURE WORK

Software for automatic analysis of FM-CW reflectometry data on NSTX has been developed and is being used to analyze data. The algorithm is extremely robust and large data sets can be analyzed without intervention. The code is currently run as a batch job due to the large amount of CPU time required (~ 30 min per shot on a Intel PIII-1 GHz CPU). Running multiple CPUs in parallel should allow between-shot analysis of the data. The necessary computer hardware and network topology are currently being explored.

ACKNOWLEDGMENT

This work is supported by U.S. DOE Grant No. DE-FG03-99ER54527.

- ¹S. Kubota, X. V. Nguyen, W. A. Peebles, L. Zeng, and E. J. Doyle, *Rev. Sci. Instrum.* **72**, 348 (2001).
- ²C. Neumeyer *et al.*, *Fusion Eng. Des.* **54**, 275 (2001).
- ³F. Simonet, *Rev. Sci. Instrum.* **49**, 1620 (1988).
- ⁴M. E. Manso, P. Varela, I. Nunes, J. Santos, G. D. Conway, M. Hirsch, S. Kluge, J. Stober, and CFN/IST Reflectometry and ASDEX Upgrade Teams, *Plasma Phys. Controlled Fusion* **43**, A73 (2001).
- ⁵S. A. Sabbagh *et al.*, *Nucl. Fusion* **41**, 1601 (2001).
- ⁶M. Ono *et al.*, in *Fusion Energy 1998*, Proceedings of the 17th International Conference on Fusion Energy, Yokohama, 1998, Vol. 3 [(IAEA, Vienna, 1999), p. 1135].
- ⁷S. M. Kaye *et al.*, *Fusion Technol.* **36**, 16 (1999).
- ⁸M. Ono *et al.*, *Nucl. Fusion* **40**, 557 (2000).
- ⁹K. W. Kim, E. J. Doyle, T. L. Rhodes, W. A. Peebles, C. L. Rettig, and N. C. Luhmann, Jr., *Rev. Sci. Instrum.* **68**, 466 (1997).
- ¹⁰E. J. Doyle, T. L. Rhodes, W. A. Peebles, and L. Zeng, *Rev. Sci. Instrum.* **70**, 1064 (1999).
- ¹¹L. Zeng, E. J. Doyle, T. C. Luce, and W. A. Peebles, *Rev. Sci. Instrum.* **72**, 320 (2001).
- ¹²M. A. Heald, *Plasma Phys.* **6**, 617 (1964).
- ¹³C. Laviron, A. J. H. Donne, M. E. Manso, and J. Sanchez, *Plasma Phys. Controlled Fusion* **38**, 905 (1996).
- ¹⁴A. V. Oppenheim, R. W. Schafer, and J. R. Buck in *Discrete-Time Signal Processing* (Prentice Hall, New York, 1999), p. 714.
- ¹⁵F. da Silva, M. Manso, A. Silva, and the ASDEX Upgrade Team, *Rev. Sci. Instrum.* **72**, 311 (2001).
- ¹⁶P. Varela, M. E. Manso, A. Silva, J. Fernandes, and F. Silva, *Rev. Sci. Instrum.* **66**, 4937 (1995).
- ¹⁷E. J. Doyle, N. L. Bretz, K. W. Kim, W. A. Peebles, and T. L. Rhodes, in *Diagnostics for Experimental Thermonuclear Fusion Reactor 2*, edited by P. E. Stott, G. Gorini, and E. Sindoni (Plenum, New York, 1998), p. 119.
- ¹⁸S. H. Heijnen, Ph.D. thesis, University of Utrecht, 1995.
- ¹⁹E. J. Doyle, T. Lehecka, N. C. Luhmann, Jr., W. A. Peebles, and the DIII-D Group, *Rev. Sci. Instrum.* **61**, 2986 (1990).
- ²⁰E. Mazzucato, *Rev. Sci. Instrum.* **69**, 2201 (1998).
- ²¹B. P. LeBlanc, R. E. Bell, D. C. Long, D. E. Hoffman, R. W. Palladino, and D. W. Johnson, *Rev. Sci. Instrum.* (these proceedings).